DOI: 10.18721/JPM.13203
УДК 532.517

ASSESSMENT OF RANS TURBULENCE MODELS CAPABILITIES BASED ON COMPUTATIONAL RESULTS FOR FREE CONVECTION DEVELOPING NEAR A SUDDENLY HEATED VERTICAL PLATE

A.M. Levchenya, S.N. Trunova, E.V. Kolesnik

Peter the Great St. Petersburg Polytechnic University, St. Petersburg, Russian Federation

The results of testing several RANS turbulence models in solving a problem of free air convection temporal development near the surface of a suddenly heated infinite vertical plate have been presented in the paper. The solution results with the use of the different models were compared with the literature data obtained by direct numerical simulation. Numerical solutions were carried out using the four models, two of them based on the isotropic turbulent viscosity concept and the rest ones involved solving the transport equations of the Reynolds stress tensor components. The flow and heat transfer characteristics for different stages of boundary layer development, from laminar to turbulent, were analyzed. Based on a comparison with the literature data on direct numerical simulation, conclusions about the predictive capabilities of the RANS models considered were drawn.

Keywords: free convection, RANS simulation, time-developing, direct numerical simulation, boundary layer

Citation: Levchenya A.M., Trunova S.N., Kolesnik E.V., Assessment of RANS turbulence models capabilities based on computational results for free convection developing near a suddenly heated vertical plate, St. Petersburg Polytechnical State University Journal. Physics and Mathematics. 13 (2) (2020) 25–36. DOI: 10.18721/JPM.13203

ОЦЕНКА ВОЗМОЖНОСТЕЙ RANS-МОДЕЛЕЙ ТУРБУЛЕНТНОСТИ ПО РЕЗУЛЬТАТАМ РАСЧЕТОВ СВОБОДНОЙ КОНВЕКЦИИ, РАЗВИВАЮЩЕЙСЯ ВБЛИЗИ ВНЕЗАПНО НАГРЕТОЙ ВЕРТИКАЛЬНОЙ ПЛАСТИНЫ

А.М. Левченя, С.Н. Трунова, Е.В. Колесник

Санкт-Петербургский политехнический университет Петра Великого,

Санкт-Петербург, Российская Федерация

В работе представлены результаты тестирования нескольких RANS-моделей турбулентности на примере решения задачи развития во времени свободной конвекции воздуха у поверхности внезапно нагретой безграничной вертикальной пластины. Результаты решения с использованием различных моделей сопоставлены с литературными данными, полученными методом прямого численного моделирования. Численные решения получены с применением четырех моделей, две из которых основаны на концепции изотропной турбулентной вязкости, а остальные предполагают решение уравнений переноса компонент тензора рейнольдсовых напряжений. Получены характеристики течения и теплообмена на разных стадиях развития пограничного слоя – от ламинарного режима до турбулентного. На основе сопоставления полученных результатов с данными прямого численного моделирования сделаны выводы о предсказательных возможностях рассмотренных RANS-моделей турбулентности.

Ключевые слова: свободная конвекция, RANS-моделирование, прямое численное моделирование, пограничный слой

Ссылка при цитировании: Левченя А.М., Трунова С.Н., Колесник Е.В. Оценка возможностей RANS-моделей турбулентности по результатам расчетов свободной конвекции, развивающейся вблизи внезапно нагретой вертикальной пластины // Научно-технические ведомости СПбГПУ. Физико-математические науки. 2020. Т. .13 2 №. С. 27–40. DOI: 10.18721/JPM.13203

Introduction

Free-convection flow near the surface of a vertical heated plate has long been the focus of attention because correctly predicting heat transfer in boundary layers is important for many practical applications. The Time-Developing approach considering the temporal evolution of the flow is an efficient computational method for analysis of developing boundary layers.

The approach basically consists in describing the temporal evolution of a boundary layer instead of the spatial evolution (the Spatial approach), which is usually observed in practice. Thus, time serves as a sort of coordinate axis along which the flow evolves. In contrast with other methods simulating flow evolution along the longitudinal (spatial) axis, this approach allows to significantly reduce the size of the computational domain and consequently the total computation time.

The Time-Developing approach is very popular for simulations of dynamic turbulent boundary layers on plates in axial flow [1, 2]. In particular, Ref. [1] discussed a laminar-turbulent transition in a boundary layer at high turbulence. For this purpose, Time-Developing Direct Numerical Simulation (TDDNS) was used to solve a model problem of a boundary layer evolving on an infinite plate in isoy tropic turbulent fluid of zero mean velocity, with the plate suddenly set in motion in its plane. The method was used in [3] to solve problems of free convection for the first time, while [4] presented promising and detailed computational results based on this method.

Although only DNS methods can yield the most complete data on the laminar-turbulent transition, whether semi-empirical RANS turbulence models can provide a satisfactory description of the transition is still open to question [5]. Furthermore, it is undoubtedly interesting to assess the efficiency of different turbulence models for simulations of the flow in fully developed turbulent free-convection boundary layers, both for the models based on isotropic turbulent viscosity [6] and for Reynolds stress models [7].

Notably, the choice of suitable turbulence models is especially critical for simulation of complex free-convection flows, including free-convection layers perturbed by different

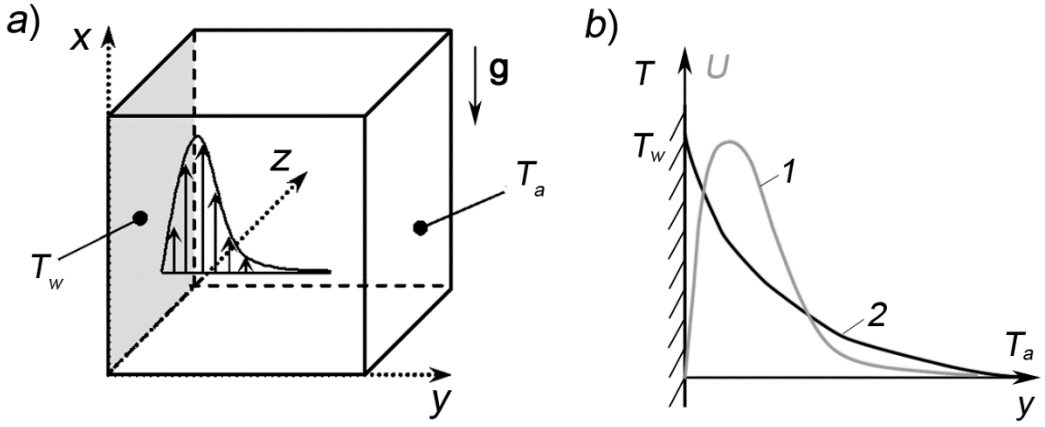

Fig. 1. Schematic for problem statement of turbulent free-convection boundary layer developing along an infinite heated vertical plate: *a* corresponds to the plate (shaded) with the surrounding ambient (cube); *b* to velocity (*1*) and temperature (*2*) distributions of the ambient air depending on the distance from the plate

kinds of obstacles. For example, [8] reports on RANS simulations (using the SST k-ω model) for flow around a cylinder of finite height mounted on a vertical heated plate, while a recent paper [9] presents simulations and experiments the same configuration.

The goal of this study consisted in assessing the performance of several RANS turbulence models by comparing the numerical solutions that we obtained with the test (reference) data from literature [4] for a model problem on the time evolution of free convection along an infinite vertical plate. We used the ANSYS Fluent 18.2 package for the computations.

TDDNS method as a source of test data

We consider a model problem of free convection developing along an infinite suddenly heated vertical plate. The flow diagram is shown in Fig. 1. The parameters of the problem in this section (described identically to [4]) correspond to the conditions of earlier well-known experiments [10] on a free-convection layer developing along a vertical plate (along the spatial coordinate). The parameters are given in Table.

The mathematical model taken for describing turbulent free convection of incompressible Newtonian fluid with constant physical properties is based on a system of unsteady 3D Navier–Stokes equations complemented with an energy balance equation, taking into account buoyancy effects in the gravity field in the Boussinesq approximation:

$$\frac{\partial u_j}{\partial x_j} = 0;$$

$$\rho\frac{\partial u_i}{\partial t} + \rho u_j\frac{\partial u_i}{\partial x_j} = -\frac{\partial p}{\partial x_i} + \frac{\partial \tau_{ij}}{\partial x_j} - \rho\beta_T\left(T - T_a\right)g_i,$$

$$i = 1,2,3; \qquad (1)$$

$$\rho c_p\frac{\partial T}{\partial t} + \rho c_p u_j\frac{\partial T}{\partial x_j} = \frac{\partial q_j}{\partial x_j}.$$

Here u_i are the components of the velocity vector $\mathbf{V}$ in Cartesian coordinates ($x \equiv x_1$, $y \equiv x_2$); p (Pa) is the pressure, T (K) is the temperature, ρ (kg/m^3) is the density and c_p (J/(kg·K)) is the heat capacity of the air.

The components of the viscous stress tensor τ and the heat flux density vector $\mathbf{q}$ due to molecular thermal conductivity are found, respectively, using Fourier's law and Newton's law of viscosity:

$$q_j = -\lambda\left(\partial T/\partial x_j\right),\ j = 1,2,3, \qquad (2)$$

$$\tau_{ij} = \mu\left(\frac{\partial u_i}{\partial x_j} + \frac{\partial u_j}{\partial x_i}\right),\ i,j = 1,2,3. \qquad (3)$$

The space shaped as a rectangular parallelepiped adjacent to the plate acts as the computational domain in TDDNS computations (Fig. 1,*a*). The outer boundary parallel to the wall is assumed to be permeable, with constant pressure p and temperature T_a given. Periodic

Table

Problem parameters

Parameter	Notation	Unit	Value
Plate temperature	T_w	K	333.15
Ambient temperature	T_a	K	289.15
Ambient density	ρ	kg/m^3	1.135
Ambient viscosity	μ	Pa·s	$1.906\cdot10^{-5}$
Ambient thermal conductivity	λ	W/(m·K)	0.0274
Heat capacity at constant pressure	c_p	J/(kg·K)	1006
Coefficient of thermal expansion	β	1/K	$3{,}458\cdot10^{-3}$
Prandtl number	Pr	–	0.71

Notes. 1. Physical properties of the air were assumed to be constant, computed at the average temperature $T_f = (T_w + T_a)/2$.
2. Coefficient β was computed at the temperature $T = T_a$.
3. Prandtl number $\mathrm{Pr} = c_p\mu/\lambda$.

conditions are imposed in homogeneous coordinates (vertical (x) and transverse (z)). After the flow fields are computed, they averaged along the homogeneous coordinates (along the x and z axes) at the next time step, so that the unsteady problem can be considered statistically one-dimensional, where the averaged parameters of the flow change only along the y axis (Fig. 1, *b*).

The notion of integral thickness of the velocity boundary layer is introduced to construct the dimensionless parameters characterizing the given flow at different instants in time. This quantity can be found by the following formula (integration with respect to y is performed over the entire ambient):

$$\delta = \int_0^\infty \frac{u}{U_m} dy. \tag{4}$$

Dimensionless temperature is also introduced:

$$\theta = \left(T - T_a\right) / \left(T_w - T_a\right). \tag{5}$$

The thickness of the temperature boundary layer δ_T is defined as the coordinate y, where $\theta = 0.01$.

The Grashof number, the Nusselt number, and the dimensionless friction constructed based on the boundary layer thickness are defined as follows:

$$\mathrm{Gr}_\delta = g\beta\Delta T\delta^3 / \nu^2, \tag{6}$$

$$\mathrm{Nu}_\delta = q_w\delta / (\lambda\Delta T), \tag{7}$$

$$\overline{\tau} = \tau_w / (\rho g\beta\Delta T\delta). \tag{8}$$

where $\Delta T = T_w - T_a$ is the temperature difference between the plate and the ambient.

Detailed data on the TDDNS model are given in [4] for the skin friction coefficient and the Nusselt number depending on the Grashof number, along with data on the mean velocity and temperature profiles and turbulence characteristics at different Gr_δ; these data are used for comparison in our study.

Problem statement based on the RANS approach

The given time-developing flow is simulated based on Reynolds-averaged Navier–Stokes equations (RANS), initially introducing averaging along homogenous coordinates (x and z). As a result, we obtain unsteady one-dimensional equations with respect to the mean axial component of velocity u and the mean temperature T:

$$\rho\frac{\partial u}{\partial t} = \frac{\partial\left(\tau_{xy} + \tau_{t,xy}\right)}{\partial y} - \rho\beta_T\left(T - T_a\right)g,$$
$$\rho c_p\frac{\partial T}{\partial t} = \frac{\partial}{\partial y}\left(q_y + q_{t,y}\right). \tag{9}$$

In this case, the transverse velocity v is taken to equal zero.

Considering the resulting unsteady one-dimensional problem, we can see that only two components of the turbulent stress tensor and the heat flux vector remain; these are $\tau_{t,xy}$ and $q_{t,y}$, reflecting turbulent transfer along a normal to the wall:

$$\tau_{t,xy} = -\rho\overline{u'v'}, \tag{10}$$

$$q_{t,y} = -\rho c_p\overline{v'T'}, \tag{11}$$

(the prime denotes the fluctuating components, the overbar denotes averaging in homogenous coordinates).

System of equations (9) is *open* in order to find a method for computing the turbulent components of the stress tensor (10) and the heat flux density vector (11). To this end, we used semi-empirical turbulence models (described below).

Notably, we obtained the solutions below using the ANSYS Fluent general-purpose code, where one-dimensional problems are solved as two-dimensional by introducing conditions for translation homogeneity. The no-slip condition and constant temperature T_w are imposed on the wall. The outer boundary parallel to the wall is assumed to be permeable with constant pressure and temperature given. Periodic conditions are imposed for the homogeneous coordinate x. It is assumed that the air has the temperature T_a at the initial time and is generally stationary. At the same time, there is initial turbulence in the region, characterized by the following parameters: turbulence intensity $I = 0.1\%$, turbulent to molecular viscosity ratio $\nu_t/\nu = 0.1$.

Turbulence models

Let us describe the general (three-dimensional) formulation of the turbulence models available in the ANSYS Fluent code that we used for our computations. These are two models based on the Boussinesq hypothesis (SST k-ω and RNG k-ε), and two Reynolds stress models (DRSM Stress-omega and DRSM StressBSL).

According to the Boussinesq hypothesis, the components of the turbulent stress tensor and the turbulent heat flux with averaged flow parameters are related as:

$$\tau_{t,ij} = \mu_t \left(\frac{\partial u_i}{\partial x_j} + \frac{\partial u_j}{\partial x_i} \right) + \frac{2}{3} k \delta_{ij}, \qquad (12)$$

$$\tau_{t,ij} = \mu_t \left(\frac{\partial u_i}{\partial x_j} + \frac{\partial u_j}{\partial x_i} \right) + \frac{2}{3} k \delta_{ij}, \qquad (13)$$

where $k = 1/2\overline{u_i' u_i'}$ is the turbulent kinetic energy, μ_t is the turbulent viscosity, λ_t is the turbulent thermal conductivity;

$$\lambda_t = c_p \mu_t / \mathrm{Pr}_t. \qquad (14)$$

Expression (14) is based on the hypothesis that the processes of turbulent transfer of momentum and heat are similar, introducing the turbulent Prandtl number Pr_t whose value is taken to be constant in the computations. The system is closed by the semi-empirical turbulence model to find the turbulent viscosity μ_t. The results below were obtained using the SST k-ω and RNG k-ε models described in [11, 12].

In case of differential Reynolds stress models, the following differential equation is solved for each of the six independent components of the Reynolds stress tensor:

$$\rho \frac{\partial}{\partial t} \overline{u_i' u_j'} + \rho u_k \frac{\partial}{\partial x_k} \overline{u_i' u_j'} = \\ = \left(D_{ij}^m + D_{ij}^t \right) + P_{ij} + \varphi_{ij} - \varepsilon_{ij}, \qquad (15)$$

where D_{ij}^m, D_{ij}^t are the terms reflecting molecular and turbulent diffusive transfer, respectively; P_{ij} is the generation term; φ_{ij} is the term responsible for redistribution of energy between tensor components, ε_{ij} is the dissipation term.

The equations for the terms related to molecular diffusion D_{ij}^m and generation P_{ij} are written as follows (no closure relations are necessary in this case):

$$D_{ij}^m = \frac{\partial}{\partial x_k} \left(\mu \frac{\partial \overline{u_i' u_j'}}{\partial x_k} \right), \qquad (16)$$

$$P_{ij} = -\rho \left[\overline{u_i' u_k'} \frac{\partial u_j}{\partial x_k} + \overline{u_j' u_k'} \frac{\partial u_i}{\partial x_k} \right]. \qquad (17)$$

As other terms of Eq. (15), D_{ij}^t, φ_{ij}, ε_{ij}, contain higher-order moments, they are computed using closures relating these terms and the averaged flow parameters.

Let us describe the specific form of the relations for the two models used in this study:

Stress-omega (referred to as DRSM SO, i.e., Differential Reynolds Stress Model Stress-Omega),

StressBSL (referred to as DRSM BSL, i.e., Differential Reynolds Stress Model Stress-BSL).

These models differ by certain closure relations and constant values.

Similar to molecular diffusion, we introduce the coefficient of turbulent diffusion proportional to turbulent viscosity for the term reflecting turbulent transfer:

$$D_{ij}^t = \frac{\partial}{\partial x_k} \left(\frac{\mu_t}{\sigma_k} \frac{\partial \overline{u_i' u_j'}}{\partial x_k} \right). \qquad (18)$$

According to the DRSM SO model, the coefficient $\sigma_k = 2$.

The coefficient σ_k un the DRSM BSL model is defined by the relation

$$\sigma_k = F_1 \sigma_{k,1} + (1 - F_1) \sigma_{k,2}. \qquad (19)$$

where $\sigma_{k,1} = 2.0$, $\sigma_{k,2} = 1.0$, and function F_1 is defined using the formulas:

$$F_1 = \tanh\left(\Phi_1^4 \right), \qquad (20)$$

$$\Phi_1 = \min \left[\max \left(\frac{\sqrt{k}}{0.09 \omega y}, \frac{500\mu}{\rho y^2 \omega} \right) \frac{4\rho k}{\sigma_{\omega,2} D_\omega^+ y^2} \right], \qquad (21)$$

$$D_\omega^+ = \max \left(2\rho \frac{1}{\omega} \frac{\partial k}{\partial x_j} \frac{\partial \omega}{\partial x_j}, 10^{-10} \right), \qquad (22)$$

$$\sigma_{\omega,2} = 1.168,$$

where y is the distance to the wall.

The term responsible for redistribution of energy between tensor components has the following form:

$$\varphi_{ij} = -C_1 \rho \beta_{RSM}^* \omega \left[\overline{u_i' u_j'} - 2/3 \delta_{ij} k \right] - \\ - \hat{\alpha}_0 \left[P_{ij} - 1/3 P_{kk} \delta_{ij} \right] - \\ - \hat{\beta}_0 \left[D_{ij} - 1/3 P_{kk} \delta_{ij} \right] - k \hat{\gamma}_0 \left[S_{ij} - 1/3 S_{kk} \delta_{ij} \right], \qquad (23)$$

$$D_{ij} = -\rho \left[\overline{u_i' u_k'} \frac{\partial u_k}{\partial x_j} + \overline{u_j' u_k'} \frac{\partial u_k}{\partial x_i} \right], \qquad (24)$$

$$S_{ij} = \frac{1}{2} \left[\frac{\partial u_j}{\partial x_i} + \frac{\partial u_i}{\partial x_j} \right]. \qquad (25)$$

The coefficient β^*_{RSM} is defined as follows for the DRSM SO model:

$$\beta^*_{RSM} = \beta^* f^*_\beta, \ \beta^* = 0.09, \tag{26}$$

$$f^*_\beta = \begin{cases} 1, \ \chi_k \le 0 \\ \dfrac{1+640\chi_k^2}{1+400\chi_k^2}, \ \chi_k > 0 \end{cases}, \tag{27}$$

$$\chi_k = \frac{1}{\omega^3}\frac{\partial k}{\partial x_j}\frac{\partial \omega}{\partial x_j}. \tag{28}$$

The coefficient $\beta^*_{RSM} = \beta^*$ for the DRSM BSL model.

The rest of the constants are given using the following formulas (identical for both models):

$$\hat{\alpha}_0 = \frac{8+\tilde{N}_2}{11}, \ \hat{\beta}_0 = \frac{8\tilde{N}_2 - 2}{11}, \quad \hat{\gamma}_0 = \frac{60\tilde{N}_2 - 4}{55}, \tag{29}$$

where $C_1 = 1.80$, $C_2 = 0.52$. (30)

The dissipation term is calculated by introducing an additional scalar variable, the specific dissipation ω:

$$\varepsilon_{ij} = 2/3\,\delta_{ij}\rho\beta^*_{RSM}k\omega. \tag{31}$$

The value of the constant β^*_{RSM} is found in the same manner as for the term φ_{ij} (see Eqs. (26)–(28)).

The turbulent kinetic energy is calculated as follows:

$$k = 1/2\,\overline{u_i' u_i'}. \tag{32}$$

Turbulent viscosity is calculated by the following formula:

$$\mu_t = \alpha^* \frac{\rho k}{\omega}, \ \alpha^* = 1. \tag{33}$$

We need to define specific dissipation ω to close the system. For this purpose, the differential transport equation for ω is solved together with the equations for the components of the Reynolds stress tensor (15). According to the DRSM SO model, this equation is written as

$$\rho\frac{\partial \omega}{\partial t} + \rho u_k \frac{\partial \omega}{\partial x_k} = \frac{\partial}{\partial x_k}\left(\Gamma_\omega \frac{\partial \omega}{\partial x_k}\right) + G_\omega - Y_\omega + S_\omega, \tag{34}$$

$$\Gamma_\omega = \mu + \mu_t/\sigma_\omega, \ \sigma_\omega = 2. \tag{35}$$

The terms G_ω, Y_ω, S_ω are found in accordance with the k-ω turbulence model [13].

According to the DRSM BSL model, an additional (cross-diffusion) term is added to Eq. (34) with respect to ω:

$$D_\omega = 2(1-F_1)\rho\frac{1}{\omega\sigma_{\omega,2}}\frac{\partial k}{\partial x_j}\frac{\partial \omega}{\partial x_j}, \tag{36}$$

where the values of the function F_1 are calculated by Eqs. (20)–(22).

The remaining terms are calculated in accordance with the BSL k-ω turbulence model.

The gradient hypothesis (13), (14) is used to calculate the turbulent heat flux components required to close the averaged energy equation; the turbulent Prandtl number is taken equal to 0.85.

Computational aspects

The computational domain is a rectangle on the xy plane. Its outer boundary is located 0.5 m away from the plate. The computational grid contained 200 cells along the y axis and 5 cells along the homogenous coordinate x. The grid was refined towards the plate surface to provide values less than unity for the dimensionless distance y^+ from the center of the first near-wall cell to the wall for the entire computational time. The time step dt was taken equal to 0.005 s. To analyze the influence of the time step on the computational results, we also performed computations where the time step was twice as short.

The computations were run in the ANSYS Fluent 18.2 package. We used the non-iterative fractional step method to advance in time.

At the stage of preliminary computations, we analyzed the influence of numerical factors on the quality of the solutions obtained. Fig. 2,*a* shows the time dependence of y^+ for all turbulence models. Evidently, y^+ takes values less than unity throughout the computations. Fig. 2,*b* shows the time dependences for the boundary layer thickness δ (calculated as integral thickness using Eq. (4)) for the SST k-ω model, obtained with different time steps. The differences are apparently insignificant.

Computational results and discussion

Influence of turbulence model on the growth in boundary layer thickness. Fig. 3 shows the time dependences of integral thickness of the velocity boundary layer, as well as the relationships between temperature and velocity layer thicknesses; these dependencies were obtained

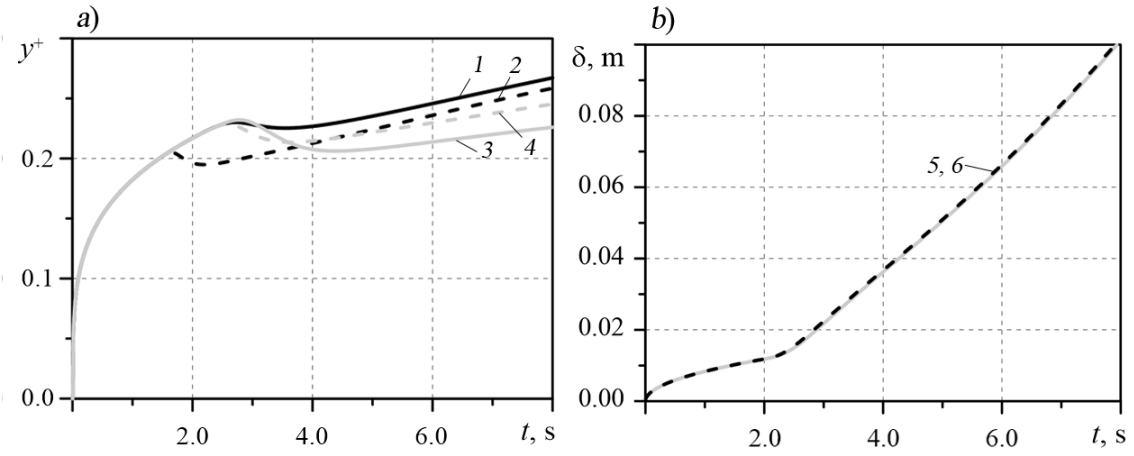

Fig. 2. Time dependences of dimensionless distance y^+ (*a*) and boundary layer thickness (*b*). Comparison of computational results obtained with different models (*a*) and influence of time step (*b*). SST *k*-ω (curve *1* and Fig. 2,*b*), RNG *k*-ε (curve *2*), DRSM SO (*3*) and DRSM BSL (*4*) models were used; time steps dt = 0.0050 (*5*) and 0.0025 s (*6*) were taken

using the given turbulence models. Fig. 3,a shows three pronounced phases in the evolution of the boundary layer: at first its thickness grows conforming to unsteady laminar layer patterns (until approximately 2 s in time), then we observe a short period with pseudo-processes of laminar-turbulent transition, and after that the boundary layer follows the turbulent flow regime (dependence of thickness δ on time is close to linear).

Comparing the results obtained using different models, we can conclude that all models yield similar predictions for the phase of laminar boundary layer (as expected), while the transition point and the peculiarities in the growth of the boundary layer in the region with developed turbulence depend on the model applied.

The DRSM SO model yields the fastest thickness growth of the turbulent velocity boundary layer, while the SST k-ω model yields the slowest growth. Apparently, the transition to turbulence (a point of characteristic change of dependences in Fig. 3) occurs simultaneously for all models except the RNG k-ε model, where this transition occurs much earlier. This model also differs by the behavior of the ratio between the temperature layer thickness and integral velocity layer thickness: while this variable reaches a nearly constant value at t > 3 s in computations by other models, it decreases over time in this model.

Comparison with the data of direct numerical simulation. We compared the obtained computational results with the TDDNS results given in [4].

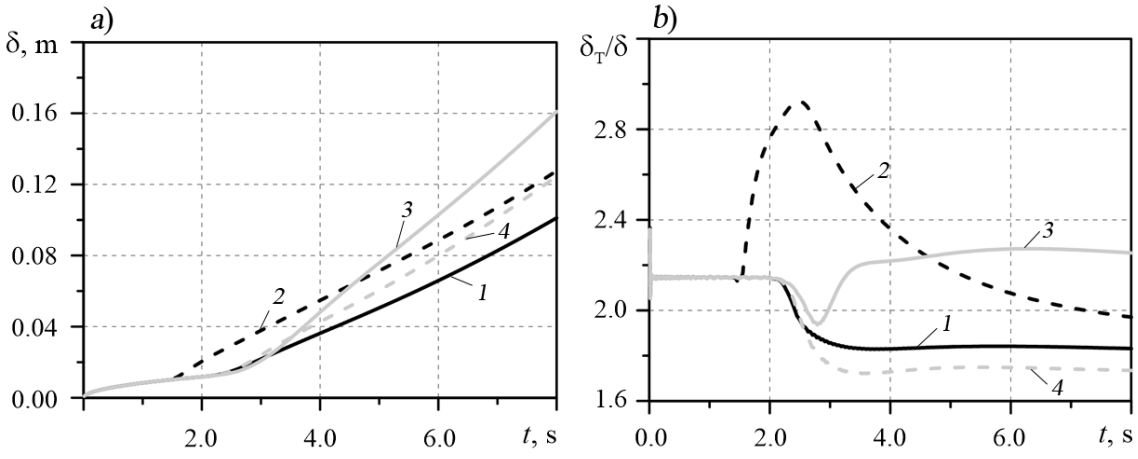

Fig. 3. Time dependences of integral thickness of velocity boundary layer (*a*) and ratios between temperature layer thickness and integral velocity layer thickness (*b*). Results are given for different models: SST *k*-ω (*1*), RNG *k*-ε (*2*), DRSM SO (*3*), DRSM BSL (*4*)

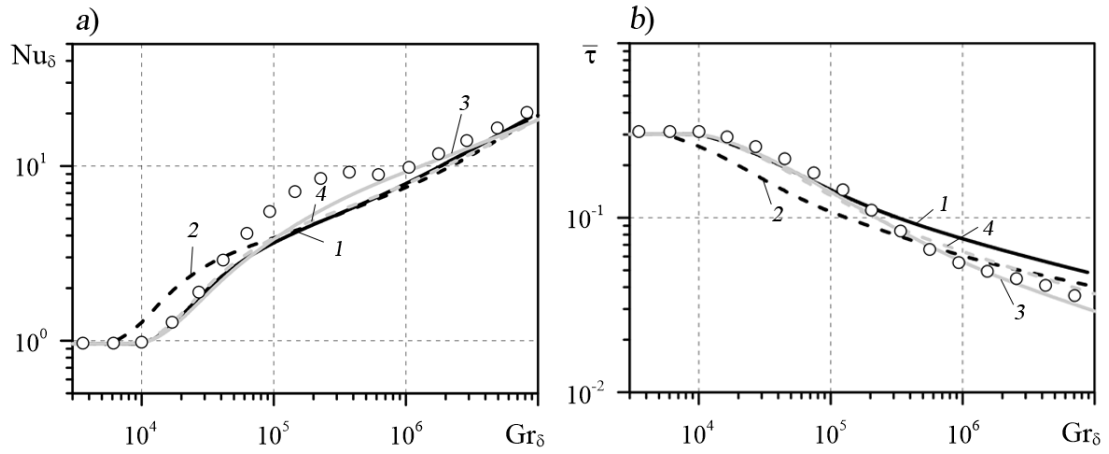

Fig. 4. Comparison of computed dependences of Nusselt number (*a*) and dimensionless friction (*b*) on Grashof number (lines) with TDDNS data (symbols);
Nu_δ and Gr_δ were constructed based on boundary layer thickness.
The curves are numbered the same as in Fig. 3

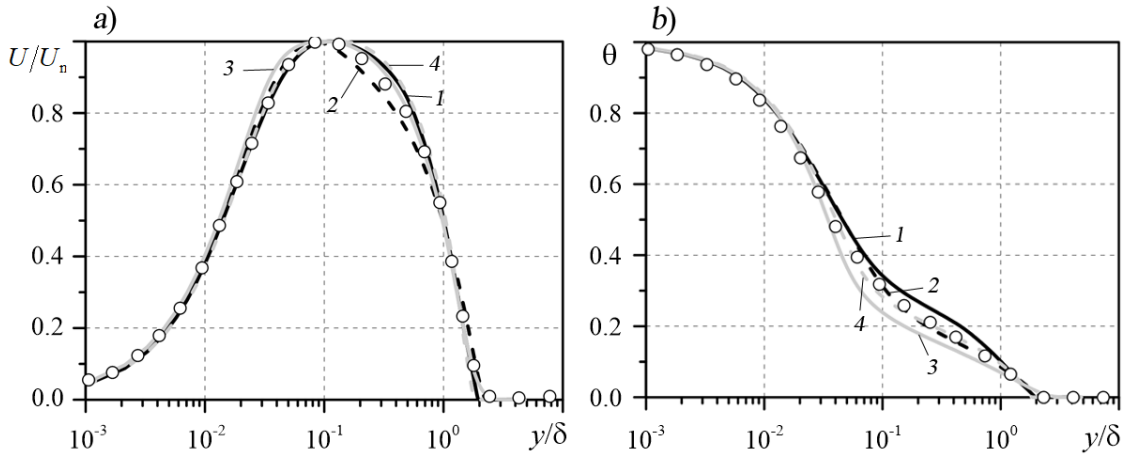

Fig. 5. Comparison of computed profiles of normalized velocity (*a*) and temperature (*b*) (lines) with TDDNS data (symbols); $Gr_\delta = 5.94 \cdot 10^6$.
The curves are numbered the same as in Figs. 3 and 4

Fig. 4 shows the dependences for the Nusselt number and the dimensionless friction on the Grashof number constructed with respect to the integral thickness of the boundary layer (see Eqs. (6)–(8)), as well as the TDDNS results. We should note that the obtained dependences differ insignificantly and are in good agreement with the TDDNS data for the stages of laminar and fully turbulent flow. However, pronounced differences appear in the behavior of the curves at the stage of transition to turbulence: direct numerical simulation predicts a local maximum for the dependence of Nu_δ on Gr_δ, while RANS simulations indicate that Nu_δ changes monotonically. Moreover, all the curves lie below the TDDNS points (a difference up to 50%). At the same time, all the dependences obtained with different models generally exhibit the same behavior in all cases, except for the earlier turbulence transition predicted by the RNG k-ε model (as mentioned above).

Analyzing the distributions of dimensionless friction over time, we found that the DRSM SO model yields the best agreement with the direct numerical simulation data, while the SST k-ω model predicts slightly overestimated values for developed turbulence.

Fig. 5 shows a comparison of the TDDNS data with the profiles of dimensionless velocity and temperature at $Gr_\delta = 5.94 \cdot 10^6$ (corresponds to the stage of developed turbulent flow). The results indicate that the velocity profiles obtained in all computations are in fairly good agreement

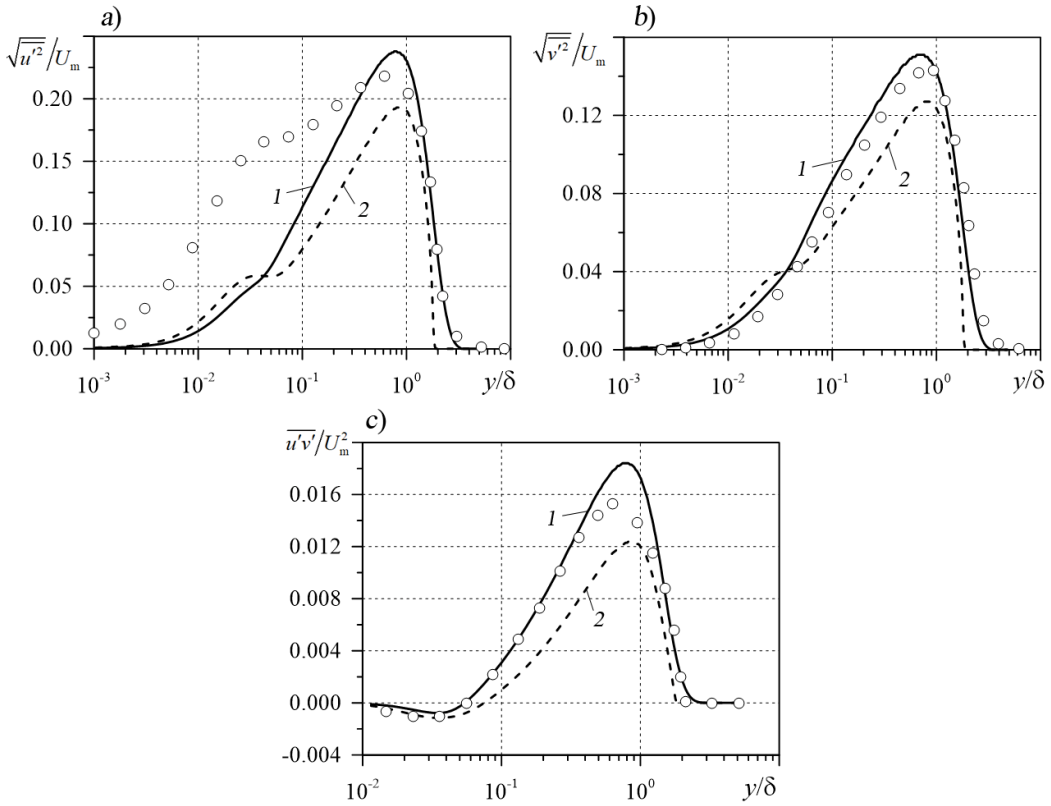

Fig. 6. Comparison of computed fluctuation intensity profiles for axial (*a*) and transverse (*b*) velocity components, and turbulent shear stress profile (*c*) (lines) with TDDNS data (symbols). Results are given for different models: DRSM SO (*1*), DRSM BSL (*2*)

with the TDDNS data. There is some divergence with TDDNS only in the outer region of the boundary layer, where velocity decreases: the RNG *k*-ε yields underestimated results, while all the other models produce overestimated ones but these discrepancies do not exceed 5%. As for the temperature distribution, DRSM BSL and RNG *k*-ε produced the best agreement with the TDDNS data. Two other models yield significant differences in the outer region of the boundary layer: the SST *k*-ω model yields a 15–20% overestimation of temperature, and the DRSM SO model a 20–25% underestimation.

Fig. 6 shows a comparison of the predicted distributions of stress tensor components along the *y* coordinate with the direct numerical simulation results for the computations performed using the Reynolds stress models (DRSM SO and DRSM BSL). The fluctuation intensity of the axial velocity component computed using both DRSM models appears to be significantly underestimated in the inner region of the boundary layer. The computed distributions of the remaining tensor components are in good agreement with the TDDNS data, with the DRSM SO model yielding the best agreement.

Conclusion

We tested two semi-empirical RANS turbulence models based on Boussinesq's hypothesis and two Reynolds stress models for the problem of free convection developing near a suddenly heated vertical plate. The results obtained by Time-Developing Direct Numerical Simulation were used as test data [4].

Analyzing the results of the computations carried out with different models, we found that the rate with which the thickness of the boundary layer grows at the stage of laminar-turbulent transition and in the developed turbulent layer phase largely depends on the model used. The DRSM SO model predicts the fastest growth in the thickness of the velocity turbulent boundary layer, while the SST k-ω model predicts the slowest growth rate.

The predictions for the dependences of the Nusselt number and the normalized friction on the Grashof number constructed based on the characteristic thickness of the growing layer are in good agreement with the TDDNS data for the stages of laminar and fully turbulent flow; the results obtained with different models differ insignificantly in this case. The DRSM SO

model yields a slightly better agreement with the TDDNS data for dimensionless friction.

The normalized velocity profiles computed for the turbulent layer phase are in a good agreement with the TDDNS data for all models considered. Analysis of the temperature profiles revealed that DRSM BSL and RNG k-ε are in best agreement with the test data. The DRSM SO and SST k-ω models give significant differences in the outer region of the boundary layer (around 20 %).

The DRSM models give fairly accurate predictions for the profiles of turbulent shear stress and fluctuation intensity of the transverse velocity component but the fluctuation intensity predicted for the axial velocity component turns out to be significantly underestimated in the inner region of the boundary layer.

The computations and analysis of the results allow to conclude that the DRSM SO model is capable of providing the best agreement with the test data [4] , obtained using the TDDNS method out of all the RANS turbulence models under consideration.

The study was sponsored by Russian Science Foundation Grant no. 18-19-00082.

REFERENCES

1. **Ustinov M.V.,** Numerical modeling of laminar-turbulent transition in a boundary layer at a high freestream turbulence level, Fluid Dynamics. 41 (6) (2006) 923–937.

2. **Huang Z.F., Zhou H., Luo J.S.,** Direct numerical simulation of a supersonic turbulent boundary layer on a flat plate and its analysis, Science China. Ser. G: Physics, Mechanics & Astronomy. 48 (5) (2005) 626 – 640.

3. **Tsuji T., Kajitani T.,** Turbulence characteristics and heat transfer enhancement of a natural convection boundary layer in water along a vertical plate, Proceedings of the 13th International Heat Transfer Conference (IHTC-13). Sydney, Australia, August 13–18. 2006. USA: Bigell House Inc, 2006.

4. **Abedin M.Z., Tsuji T., Hattori Y.,** Direct numerical simulation for a time-developing natural-convection boundary layer along a vertical plate, International Journal of Heat and Mass Transfer. 52 (19–20) (2009) 1723–1734.

5. **Abdollahzadeh M., Esmaeilpour M., Vizinho R., et al.,** Assessment of RANS turbulence models for numerical study of laminar-turbulent transition in convection heat transfer, International Journal of Heat and Mass Transfer. 115, B (December) (2017) 1288–1308.

6. **Henkes R.A.W.M., Hoogendoorn C.J.,** Comparison of turbulence models for the natural convection boundary layer along a heated vertical plate, International Journal of Heat and Mass Transfer. 32 (1) (1989) 157–169.

7. **Peeters T.W.J., Henkes R.A.W.M.,** The Reynolds-stress model of turbulence applied to the natural-convection boundary layer along a heated vertical plate, International Journal of Heat and Mass Transfer. 35 (2) (1992) 403–420.

8. **Smirnov E.M., Levchenya A.M., Zhukovskaya V.D.,** RANS-based numerical simulation of the turbulent free convection vertical-plate boundary layer disturbed by a normal-to-plate circular cylinder, International Journal of Heat and Mass Transfer. 144 (December) (2019) 118573.

9. **Chumakov Yu.S., Levchenya A.M., Khrapunov E.F.,** An experimental study of the flow in the area of influence of a cylinder immersed in the free convective boundary layer on a vertical surface, St. Petersburg State Polytechnical University Journal. Physics and Mathematics. 13 (1) (2020) 66–77.

10. **Tsuji T., Nagano Y.,** Characteristics of a turbulent natural convection boundary layer along a vertical flat plate, International Journal of Heat and Mass Transfer. 31 (8) (1988) 1723–1734.

11. **Menter F.R., Kuntz M., Langtry R.,** Ten years of industrial experience with the SST turbulence model turbulence, Turbulence, Heat and Mass Transfer, Vol. 4. Proceedings of the Fourth International Symposium on Turbulence, Heat and Mass Transfer, Antalya, Turkey, 12–17 October, 2003, Pp. 625–632.

12. **Orszag S.A., Yakhot V., Flannery W.S., et al.,** Renormalization group modeling and turbulence simulations, In: Proceedings of the International Conference on Near-Wall Turbulent Flows, Tempe, Arizona, USA, 15–17 March (1993) 1031.

13. **Wilcox D.C.,** Turbulence modeling for CFD, 2nd edition, DCW Industries, Inc. La Canada, California, 1998.

14. **Menter F.R.,** Two-equation eddy-viscosity turbulence models for engineering applications, AIAA Journal. 32 (8) (1994) 1598–1605.

Received 31.03.2020, accepted 29.04.2020.

THE AUTHORS

LEVCHENYA Alexander M.
Peter the Great St. Petersburg Polytechnic University
29 Politechnicheskaya St., St. Petersburg, 195251, Russian Federation
levchenya_am@spbstu.ru

TRUNOVA Seraphima N.
Peter the Great St. Petersburg Polytechnic University
29 Politechnicheskaya St., St. Petersburg, 195251, Russian Federation
seraphimatr@yandex.ru

KOLESNIK Elizaveta V.
Peter the Great St. Petersburg Polytechnic University
29 Politechnicheskaya St., St. Petersburg, 195251, Russian Federation
kolesnik_ev@mail.ru

СПИСОК ЛИТЕРАТУРЫ

1. **Устинов М.В.** Численное моделирование ламинарно-турбулентного перехода в пограничном слое при повышенной степени турбулентности потока // Известия РАН. Механика жидкости и газа. 2006. № 6. С. 77–93.

2. **Huang Z.F., Zhou H., Luo J.S.** Direct numerical simulation of a supersonic turbulent boundary layer on a flat plate and its analysis // Science China. Ser. G: Physics, Mechanics & Astronomy. 2005. Vol. 48. No. 5. Pp. 626–640.

3. **Tsuji T., Kajitani T.** Turbulence characteristics and heat transfer enhancement of a natural convection boundary layer in water along a vertical plate // Proceedings of the 13th International Heat Transfer Conference (IHTC-13). Sydney, Australia, August 13–18. 2006. USA: Bigell House Inc, 2006.

4. **Abedin M.Z., Tsuji T., Hattori Y.** Direct numerical simulation for a time-developing natural-convection boundary layer along a vertical plate // International Journal of Heat and Mass Transfer. 2009. Vol. 52. No. 19–20. Pp. 1723–1734.

5. **Abdollahzadeh M., Esmaeilpour M., Vizinho R., Younesi A., Pascoa J.C.** Assessment of RANS turbulence models for numerical study of laminar-turbulent transition in convection heat transfer // International Journal of Heat and Mass Transfer. 2017. Vol. 115. Part B. December. Pp. 1288–1308.

6. **Henkes R.A.W.M., Hoogendoorn C.J.** Comparison of turbulence models for the natural convection boundary layer along a heated vertical plate // International Journal of Heat and Mass Transfer. 1989.Vol. 32. No. 1. Pp. 157–169.

7. **Peeters T.W.J., Henkes R.A.W.M.** The Reynolds-stress model of turbulence applied to the natural-convection boundary layer along a heated vertical plate // International Journal of Heat and Mass Transfer. 1992. Vol. 35. No. 2. Pp. 403–420.

8. **Smirnov E.M., Levchenya A.M., Zhukovskaya V.D.** RANS-based numerical simulation of the turbulent free convection vertical-plate boundary layer disturbed by a normal-to-plate circular cylinder // International Journal of Heat and Mass Transfer. 2019. Vol. 144. December. P. 118573.

9. **Чумаков Ю.С., Левченя А.М., Храпунов Е.Ф.** Экспериментальное исследование течения в зоне влияния цилиндра, погруженного в свободноконвективный пограничный слой на вертикальной поверхности // Научно-технические ведомости СПбГПУ. Физико-математические науки. 2020. Т. 13. № 1. С. 66–77.

10. **Tsuji T., Nagano Y.** Characteristics of a turbulent natural convection boundary layer along a vertical flat plate // International Journal of Heat and Mass Transfer. 1988. Vol. 31. No. 8. Pp. 1723–1734.

11. **Menter F.R., Kuntz M., Langtry R.** Ten years of industrial experience with the SST turbulence model // Turbulence, Heat and Mass Transfer. Vol. 4. Proceedings of the Fourth International Symposium on Turbulence, Heat and Mass Transfer. Antalya, Turkey. 12–17 October, 2003. Pp. 625–632.

12. **Orszag S. A., Yakhot V., Flannery W. S., Boysan F., Choudhury D., Maruzewski J., Patel B.** Renormalization group modeling and turbulence simulations // Proceedings of

the International Conference on Near-Wall Turbulent Flows, Tempe, Arizona, USA., 15–17 March 1993. P. 1031.

13. **Wilcox D.C.** Turbulence modeling for CFD. 2nd edition. La Canada, California: DCW Industries, 1998. 457 p.

14. **Menter F. R.** Two-equation eddy-viscosity turbulence models for engineering applications // AIAA Journal. 1994. Vol. 32. No. 8. Pp. 1598–1605.

Статья поступила в редакцию 31.03.2020, принята к публикации 29.04.2020.

СВЕДЕНИЯ ОБ АВТОРАХ

ЛЕВЧЕНЯ Александр Михайлович – *кандидат физико-математических наук, доцент Высшей школы прикладной математики и вычислительной физики Санкт-Петербургского политехничее ского университета Петра Великого, Санкт-Петербург, Российская Федерация.*

195251, Российская Федерация, г. Санкт-Петербург, Политехническая ул., 29
levchenya_am@spbstu.ru

ТРУНОВА Серафима Николаевна – *студентка магистратуры Института прикладной математики и механики Санкт-Петербургского политехнического университета Петра Великого, Санкт-Петербург, Российская Федерация.*

195251, Российская Федерация, г. Санкт-Петербург, Политехническая ул., 29
seraphimatr@yandex.ru

КОЛЕСНИК Елизавета Владимировна – *ассистент Высшей школы прикладной математики и вычислительной физики Санкт-Петербургского политехнического университета Петра Великого, Санкт-Петербург, Российская Федерация.*

195251, Российская Федерация, г. Санкт-Петербург, Политехническая ул., 29
kolesnik_ev@mail.ru